Neuroscience 123 (2004) 231–245

SIMPLE AND COMPLEX VISUAL MOTION RESPONSE PROPERTIES IN THE ANTERIOR MEDIAL BANK OF THE LATERAL SUPRASYLVIAN CORTEX

B. G. OUELLETTE,[a,b] K. MINVILLE,[a] J. FAUBERT[a] AND C. CASANOVA[a]*

[a]*Visual Neuroscience Laboratory, School of Optometry, Université de Montréal, CP 6128, Succ. Centre-ville, Montréal, Quebec, Canada H3C 3J7*

[b]*Département de Psychologie, Université de Montréal, Montréal, Quebec, Canada H3C 3J7*

Abstract—The cortical regions surrounding the suprasylvian sulcus have previously been associated with motion processing. Of the six areas originally described by Palmer et al. [J Comp Neurol 177 (1978) 237], the posteromedial lateral suprasylvian (PMLS) cortex has attracted the greatest attention. Very little physiological information is available concerning other suprasylvian visual areas, and in particular, the anteromedial lateral suprasylvian cortex (AMLS). Based on its cortical and sub-cortical connectivity patterns, the AMLS cortex is a likely candidate for higher-order motion processing in cat visual cortex. We have investigated this possibility by studying the receptive field sensitivity of AMLS neurons to complex motion stimuli. Neurons in AMLS cortex exhibited large (mean of 354°^{2}) and complex-like receptive fields, and most of them (74%) were classified as direction selective on the basis of their responses to sinusoidal drifting gratings. Most importantly, direction selectivity was present for complex motion stimuli. A subset of the neurons sampled (eight of 38 cells; 21%) exhibited pattern-motion selectivity in response to moving plaid patterns. The capacity of AMLS neurons to signal higher-order stimuli was further supported by their selectivity to moving complex random-dot kinematograms. Finally, 45% of 20 neurons were direction selective to a radial optic flow stimulus. Overall, these results suggest that AMLS cortex is involved in higher-order analyses of visual motion. It is possible that the AMLS cortex represents a region between PMLS and the anterior ectosylvian visual area in a functional hierarchy of areas involved in motion integration.

Key words: electrophysiology, plaid patterns, random dot kinematograms, optic flow, direction selectivity, functional hierarchy.

Locomotion and the displacement of objects within the environment create complex visual motion cues that must be properly analyzed by the brain to permit appropriate visuo-motor behavior. In cats, the cortical areas lying in the medial, lateral, and ventral banks of the suprasylvian sulcus are believed to be crucial for the analysis of motion. This is especially true of the most extensively studied posteromedial part of the lateral suprasylvian (PMLS) cortex. On the basis of neuronal response properties and behavioral observations, PMLS has been associated with simple and complex motion analysis (Rauschecker, 1988; Spear, 1991; Dreher et al., 1996).

Very little, if anything, is known about the visual response properties of neurons in the five other areas surrounding the suprasylvian sulcus as defined by Palmer et al. (1978; see Spear 1991). In particular, very few studies have concentrated on the anteromedial part of the lateral suprasylvian (AMLS) cortex. This region receives convergent inputs from extrastriate areas and thalamic structures involved in complex motion processing: the PMLS cortex (Symonds and Rosenquist, 1984a,b; Norita et al., 1996), the anterior ectosylvian visual (AEV) area (Reinoso-Suárez and Roda, 1985; Norita et al., 1986; Olson and Graybiel, 1987; Norita et al., 1996; but see Symonds and Rosenquist, 1984a), and the lateral posterior nucleus-pulvinar complex (LP-pulvinar; Symonds et al., 1981; Updyke, 1981; Tong et al., 1982; Raczkowski and Rosenquist, 1983; Norita et al., 1996). Therefore, on the basis of its connectivity, the AMLS cortex may play a key role in motion analysis. However, this statement cannot be substantiated by electrophysiological data given the lack of information regarding receptive field properties in this part of the lateral suprasylvian cortex. To our knowledge, only two neurophysiological studies specifically targeted the AMLS cortex. Toyama et al. (1990) reported that neurons in this area could be visually driven by looming objects. Yaka et al. (2002) subsequently found an equal proportion of visual and auditory neurons, and reported that a subset of units were bimodal. Behavioral assessments further suggested that AMLS cortex is involved in visual processing, namely the discrimination of stimulus orientation, direction and spatial landmarks (Lomber, 2001; Vanduffel et al., 1997; Sprague et al., 1996).

Based on the connectivity pattern of AMLS cortex with cortical and subcortical regions involved in higher-order motion processing, we investigated whether AMLS neurons could signal complex motion. On the basis of the neuronal response characteristics in AMLS cortex to complex motion stimuli, it may be possible to suggest where AMLS cortex should be situated in a functional hierarchy of visual areas involved in the analysis of motion cues. Be-

*Corresponding author. Tel: +1-514-343-2407; fax: +1-514-343-2382.
E-mail address: christian.casanova@umontreal.ca (C. Casanova).

Abbreviations: AEV, anterior ectosylvian visual area; AMLS, anteromedial lateral suprasylvian cortex; CM, component motion; DI, direction index; LP-pulvinar, lateral posterior nucleus–pulvinar complex; MI, modulation index; PM, pattern motion; PMLS, posteromedial lateral suprasylvian cortex; PSTH, peri-stimulus time histogram; RDK, random dot kinematogram.

0306-4522/04$30.00+0.00 © 2003 IBRO. Published by Elsevier Ltd. All rights reserved.
doi:10.1016/j.neuroscience.2003.09.002

cause of the general lack of knowledge about AMLS visual physiology, we also studied some basic receptive field properties. Parts of these findings have been presented elsewhere in abstract form (Minville et al., 1997; Ouellette et al., 2001).

EXPERIMENTAL PROCEDURES

Animal preparation

Eighteen normal adult cats weighing between 2.5 and 4.5 kg were used. All procedures were in accordance with the guidelines set out by the Canadian Council on Animal Care and were approved by the ethical committee on animal research of the Université de Montreal. All efforts were made to minimize animal suffering and to reduce the number of animals used. Animals were pre-anesthetized with a s.c. injection of acepromazine (1 mg/kg) and atropine (0.1 mg/kg). General anesthesia was induced via a mask with a gaseous mixture of Isoflurane (2–5%), with N_2O/O_2 (50/50%). Cardiac rhythm and O_2 saturation were monitored with an oxymeter. A local anesthetic (lidocaine hydrochloride 2%) was applied to incision and pressure points. Tracheotomy and cannulation of the cephalic vein were performed before transferring the animal to the stereotaxic apparatus. The cannula allowed for the administration of gallamine triethiodide (10 mg/kg/h) delivered in lactated Ringers solution. The animal was then artificially ventilated with N_2O/O_2 (70/30%) and halothane (0.5–1%). Levels of CO_2 were maintained between 28 and 32 mm Hg by adjusting the stroke volume and respiratory rate. Rectal temperature was monitored and maintained at approximately 37.5 °C. Electrocardiogram and electroencephalogram were continuously monitored. Pupils were dilated and nictitating membranes retracted with atropine (1%) and phenylephrine hydrochloride (2.5%) respectively. The eyes were then protected with contact lenses with the appropriate refractive power. Craniotomies were performed bilaterally at Horsley-Clarke coordinates anterior: 8–14 and lateral: 11–16, and the dura was reflected. The electrode was angled in a coronal plane approximately 40° with respect to vertical and lowered along the medial bank of the suprasylvian sulcus. The cortex was covered with warm agar and melted wax in order to create a sealed chamber.

Recordings

Varnished tungsten microelectrodes (A&M Systems, Carlsborg, WA, USA; impedance between 1.5 and 4.0 mΩ), were used to record extracellular single-unit activity in AMLS cortex. Neuronal activity was amplified, displayed on an oscilloscope, and played through an audio monitor. A window discriminator was used to isolate single units from the overall signal and the waveforms of the action potentials were routinely examined. Digital signals were then fed to acquisition software (Spike2; CED, Cambridge, UK) via an analog-digital interface (CED 1401 plus). The response for each stimulus condition was recorded as a peri-stimulus time histogram (PSTH) (bin width of 10 ms) and was saved for further statistical analysis. Recording for a single trial occurred over a 4 s period and mean firing frequency was calculated from all 400 bins and averaged over several presentations (at least four).

Visual stimulation

Receptive fields were mapped by hand on a tangent screen subtending 80°×107° of visual angle, using an ophthalmoscope that could present circles up to 12° diameter. A hand held projector was used to present large rectangles (approximately 10°×2°). In the early phase of the study, visual stimuli (sine wave gratings, plaid patterns, and Julesz-type noise), were generated by the Picasso Image generator (Innisfree) controlled by the software package Visual Stimulation (VS) v1.72 (CED, Cambridge, UK). Stimuli were presented on a CRT display (5117, Data Check, Van Nuys, CA, USA; mean luminance 14cd/m^2) placed 57 cm in front of the animal. The screen subtended 28°×28° of visual angle and stimuli covered the entire display. The CRT was placed so as to align its center with that of the receptive field. Julesz-type texture patterns (hereafter visual noise) were generated by a Dual Velocity Field and Stereogram Generator (Innisfree) connected to the Picasso Image generator (see below). In later experiments, stimuli were generated by a Macintosh G3 computer using VPixx 1.5 (Sentinel Medical Research, Ste-Julie, Quebec, Canada) and back-projected onto a tangent screen (80°×107°) placed 57 cm in front of the animal. Stimuli covered 75°×92°, regardless of the size of the receptive field. The screen was not displaced unless a receptive field border fell outside of the area that could be stimulated: this was very unusual given that almost all receptive fields were located in the binocular zone of the visual field (see Fig. 2B, almost all receptive fields are within 20° of eccentricity). The screen (Da-Lite) consists of a special coat applied to an acrylic substrate (Da-Plex) that permits a uniform distribution of the light projected onto the screen. Stimuli were displayed at a frame rate of 67 Hz and had a mean luminance of 25 cd/m^2. The VPixx system allowed the generation of more complex stimuli such as random dot kinematograms (RDKs) and radial optic flow fields (see below).

A subset of nine cells was tested with both stimulation systems, using the same range of values. For this subset of cells, optimal properties and tuning widths were similar when the values tested with VPixx were limited to those tested with VS. The VS system did not allow the generation of drifting gratings at spatial frequencies below 0.05 c/°. Some cells considered as low-pass units with VS may have been band-pass tuned and optimally responsive to lower spatial frequency values. Therefore, spatial frequency data obtained with the VS system is presented briefly for the purpose of comparison with our previous studies in other regions that had the same technical limitation (e.g. Merabet et al., 2000).

Receptive field size and binocular dominance were first assessed qualitatively. In a majority of cases, one eye was found to be clearly dominant and monocular stimulation was performed. When neuronal responses could not be driven by monocular stimulation, binocular presentations were used. In that condition, no alignment of the eyes was made because receptive fields of the two eyes could not be mapped individually. Thereafter, drifting sinusoidal gratings (60% contrast) were used to quantitatively determine direction-selectivity, and spatial and temporal contrast sensitivity. Direction was varied over 360° in 12 or 24 steps of 30° or 15°, respectively. Spatial frequency tuning was assessed using gratings drifted at the preferred direction and temporal frequency (the latter being first qualitatively assessed). Temporal frequency tuning was then quantitatively determined using a drifting grating at the preferred direction and optimal spatial frequency. Subsequently, a direction tuning function was assessed a second time to insure that direction selectivity was still present despite the low spatial frequencies.

Visual noise patterns consisted of a grid of black and white elements. Each element subtended 0.13° of visual angle and represented the outcome of an independent Bernoulli trial with equiprobable states. These stimuli were used as they are purely directional stimuli; two-dimensional Fourier power spectrum analysis revealed that all orientations are equally represented in both frequency axes, as are all spatial frequencies up to 128 cycles/image (see Fig. 1 in Merabet et al., 2000). Moreover, this stimulus has been used in other visual areas (Casanova et al., 1995; Casanova and Savard, 1996; Merabet et al., 2000), thus it allows a direct comparison of the responses of neurons in AMLS cortex with those areas. Movement of the stimulus consisted of a translation of the entire visual noise pattern. Both the direction and

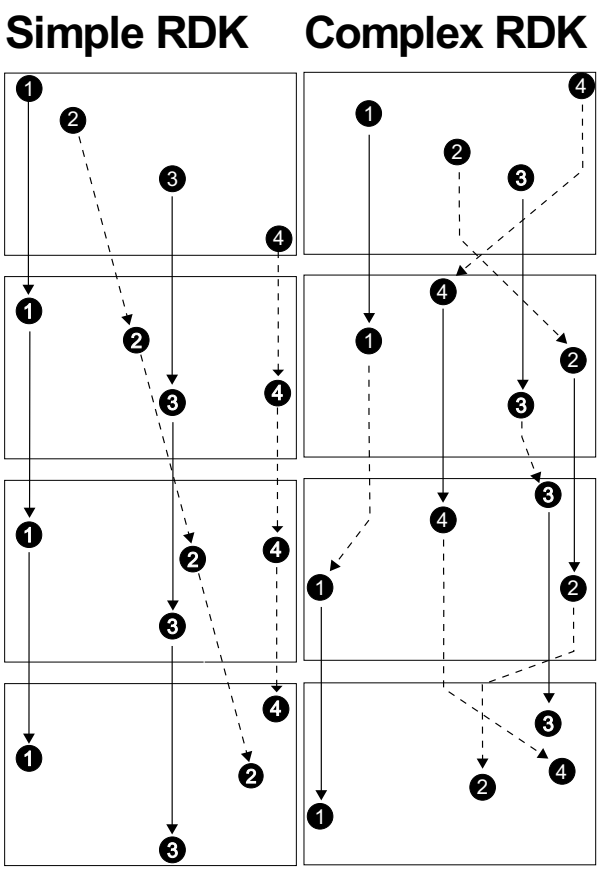

Fig. 1. Schematic of the simple and complex RDKs. Solid lines represent motion signals while dashed lines illustrate the displacement of the noise dots. Each rectangle equals one stimulus frame. Note that there is an equal number of signal and noise displacements for simple and complex RDKs.

speed that elicited an optimal response were assessed. A more detailed description of the stimulus can be found in Merabet et al. (2000).

For a subset of direction-selective cells, responses to drifting plaid patterns were assessed. Plaids were composed of two superimposed sinusoidal gratings of identical spatial and temporal frequency that drifted in directions that differed by 120°. The spatial and temporal frequencies used for each component grating were determined for each neuron individually, according to the optimal values previously identified with drifting gratings. The contrast of each grating was 30%, so that the total contrast of the plaid was equivalent to that of a single drifting grating.

RDKs consisting of white circular dots (1° diameter, 100% contrast) on a black background were used to study global motion processing. To be consistent with previous findings (Dumbrava et al., 2001), these RDKs will be referred to as simple and complex. A diagram of each type of RDK is presented in Fig. 1. The simple RDK was essentially a rigidly translating random dot field with 50% noise (coherence was set to 50% to allow a direct comparison with complex RDK responses; see below). In this configuration, each signal dot follows a straight and continuous path in one common direction. Noise dots followed trajectories along randomly chosen directions, and occasionally crossed the path of signal dots. This stimulus required minimal simultaneous motion integration over an area of the visual field.

For complex RDKs, the dots had a lifetime of two frames, that is, they moved only once before being randomly repositioned, i.e. being displaced to another location. Each dot had an equal and random probability of beginning as a signal dot on even- or odd-numbered frames. At any one time, half of the dots were displaced in the motion direction while the remaining half were repositioned randomly. In other words, the signal and noise frames have been segmented by half, so that when half of the dots give the motion signals, the remaining dots repositioned themselves (the reverse being observed in the next sequence). In the complex RDK, there is never more than a single coherent motion before repositioning. Consequently, there must be a spatial and temporal integration of the displacement of many dots over an extended area of the visual field in order to signal the veridical direction of the pattern. Unlike the simple RDK, it is impossible to extract the overall direction of a complex RDK by tracking a single signal dot. It has been shown that neurons in area 17 are not direction-selective to this stimulus (Dumbrava et al., 2001; Villeneuve and Casanova, 2001), supporting its complex nature.

Optic flow, designed to mimic the motion of an observer traveling through a tunnel, consisted of white trapezoids on a black background (100% contrast). The trapezoids followed radial trajectories originating from a point that was centered on the area centralis, whose position was calculated from optic nerve mapping (Bishop et al., 1962). The central 2° of the display was left blank in order to avoid clumping of the elements in that region. The stimulus was not restricted to the receptive field of the cell but rather, covered the entire display (75°×92°). Both speed and size gradients similar to those described by Gibson (1950) were present in these stimuli. Trapezoids were displayed and continued to move along a radial trajectory until they went beyond the borders of the display field. The coherence of motion was set to 100%. The direction of motion was either expanding or contracting. The acceleration of expanding and contracting motion of the elements was exponential in order to mimic natural flow field cues. Trapezoids were 2° wide and 6° long when the trailing edge was at 10° eccentricity. At this same eccentricity, the motion of the stimulus would be equivalent to a cat moving through the environment at 6.87 km/h. Parameters such as velocity and dot population were varied in order to elicit a maximal response. For a detailed description of the optic flow stimuli, see Brosseau-Lachaine et al. (2001). In order to further study the possible role of AMLS cortex in the analysis of self-motion cues, the preferred axial direction of a subset of neurons was quantified (Rauschecker et al., 1987). Axial direction preference represents the difference between the conventional directional preference of the cell and the polar angle of the receptive field center (defined as the angle of the receptive field center in polar visual-field coordinates). A preferred axial direction value close to 0° represents a centrifugal directional bias while a value close to 180° represents a centripetal direction bias of a cell.

Analysis of neuronal responses

Tuning functions were collected by testing stimuli at values on both sides of the optimal. Bandwidth for direction tuning functions was calculated as the half-width at half-height of the tuning curve, while that for spatial and temporal frequency tuning curves represented the full-width at half-height. Direction selectivity of AMLS neurons was assessed by calculating a direction index (DI) as follows:

$$DI = 1 - \frac{\text{response in the nonpreferred direction} - \text{spontaneous activity}}{\text{response in the preferred direction} - \text{spontaneous activity}}$$

Neurons with values above 0.5 were considered as direction selective, whereas cells below this value were not considered as such (Merabet et al., 2000). Data obtained with drifting sine wave gratings were used to calculate a modulation index (MI) (Skottun

et al., 1991) as follows:

$$MI = \frac{\text{response to the 1st harmonic}}{\text{mean response} - \text{spontaneous activity}}$$

The MI is an indicator of the extent to which a cell modulates its response amplitude for a given grating temporal frequency, and is traditionally used to discriminate simple from complex cells in area 17.

Responses to plaids were classified as pattern motion selective (PM) or component motion selective (CM) by calculating partial correlation coefficients using the following formula: $R_p=(r_p-r_c r_{pc})/[(1-r_c^2)(1-r_{pc}^2)]^{1/2}$ (Movshon et al., 1986, corrected). R_p represents the partial correlation coefficient for the PM prediction, r_c is the correlation coefficient of the plaid response and the CM prediction, r_p is the correlation coefficient for the plaid response and the pattern prediction, and r_{pc} is the correlation coefficient for the two predictions. Similarly, R_c is the partial correlation coefficient defined for the CM prediction and is calculated by exchanging r_p with r_c in the equation. Component and pattern predictions were based on a neuron's direction tuning function to a drifting sine wave grating. The PM prediction is identical to the cell's actual response to the grating. To obtain the CM prediction, spontaneous activity is subtracted from the cell's response to the grating. The direction tuning function is then duplicated and each copy is shifted 60° in opposite directions. Both direction tuning functions and spontaneous activity are then summed.

Cells were tested either with 12 or 24 directions, thus influencing critical values (i.e. by changing the degrees of freedom). In order to present all data in one graph, partial correlation coefficients were transformed into Z scores (Majaj et al., 1999; J. A. Movshon, personal communication). Transformations to Z scores were performed with a modified (Sokal and Rohlf, 1981) version of Fisher's transform:

$$Z_{Rp}=\frac{0.5\ \ln((1+R_p)/(1-R_p))}{\sqrt{1/(n-3)}}$$

Z_{Rc} can be calculated by replacing R_p with R_c. The n represents the number of directions at which the stimulus was presented.

A cell was considered as PM selective when the value of R_p (or Z_{Rp}) was significantly greater than R_c (or Z_{Rc}) and zero, as determined with a t-test (one tail $\alpha=0.05$). A CM selective cell has a R_c (or Z_{Rc}) that is significantly greater than R_p (or Z_{Rp}) and zero. The critical values for a statistically significant difference are plotted as solid and dashed lines in Fig. 9C, D. In panel C there are two lines representing critical values since the latter is directly influenced by the number of directions tested (12 or 24).

Histology

Electrolytic lesions were made along all penetrations to allow for reconstruction of electrode tracks. At the end of the experiments, animals were killed by intravenous administration of pentobarbital sodium (Euthanyl: 0.96 mg/kg). Brains were cut in blocks in the stereotaxic apparatus and then removed and placed in buffered formalin (10%). Frozen serial sections of AMLS cortex were cut in a coronal plane at a thickness of 40 μm. Cresyl Violet stain permitted the distinction of cortical layers. The exact position of electrode tracks was verified to be in the medial bank of the suprasylvian sulcus.

RESULTS

General observations

Recording in AMLS cortex was tedious since many neurons were not visually responsive. Only 144 of 592 neurons were considered visual when stimulated with hand-held projectors, and computer-controlled full-screen drifting sine wave gratings. Along a penetration, it was common not to encounter a single visual neuron. One cannot rule out the possibility that visual neurons in AMLS are more sensitive to anesthetic levels than those in the neighboring PMLS cortex (Merabet et al., 2000). However, the relatively low number of visual cells may simply reflect the multimodal nature of this area that is known to receive visual, auditory, visuomotor, and somatosensory afferents (Kawamura and Naito, 1980; Symonds and Rosenquist, 1984a; Norita et al., 1996). In the present study, systematic verification of the multimodal character of AMLS neurons was not carried out, but occasional qualitative verification revealed that both somatosensory and auditory cells were present, the latter being consistent with previous reports (see introduction).

All parts of AMLS cortex were sampled equally, except at the extreme rostral and caudal limits. Neurons in these two segments (A: 8–9 and A: 13–14) represent less than 9% of sampled cells. None of the visual response properties discussed below were observed to vary along the antero-posterior axis of AMLS cortex (see below for statistics).

Basic receptive field properties

For 129 of the 144 visually responsive neurons, receptive fields were hand-plotted with confidence. They were generally large and their area ranged between 44 and 1595°^{2}, with a mean of 354±276°^{2} (Fig. 2A). This value did not vary along the AMLS antero-posterior axis ($r=0.14$, $P=0.12$). Qualitative inspection of receptive fields revealed no clear segregation of ON and OFF regions. Cells responded best to brisk movement of light, regardless of size and shape. A majority of receptive fields were situated within 20° of the center of the visual field and located below the horizontal meridian (Fig. 2B). Similar to the findings of Palmer et al. (1978), receptive field positions went from the periphery to the area centralis, as the microelectrode descended along the medial bank of the cortex. However, no clear visuotopic organization, similar to that described by Palmer et al. (1978), was observed along either antero-posterior or medio-lateral axes. This may be attributable to the large receptive field size of AMLS neurons and the smaller number of penetrations performed per animal as compared with that in Palmer et al. (1978).

Motion sensitivity and direction selectivity

Sine-wave gratings. A representative example of an AMLS cell response, as a function of grating direction, is presented in Fig. 3A. This unit responded with unmodulated discharges to a fairly broad range of directions of motion. Panel B shows the corresponding tuning curve and illustrates that this neuron responded to a number of different directions on either side of the optimal. This neuron had a bandwidth of 29.8° and was strongly direction selective (DI=0.95). Note the low level of spontaneous activity (0.62 spikes/s) that was typical of AMLS neurons (sample mean=7.33±8.79 spikes/s). The distribution of

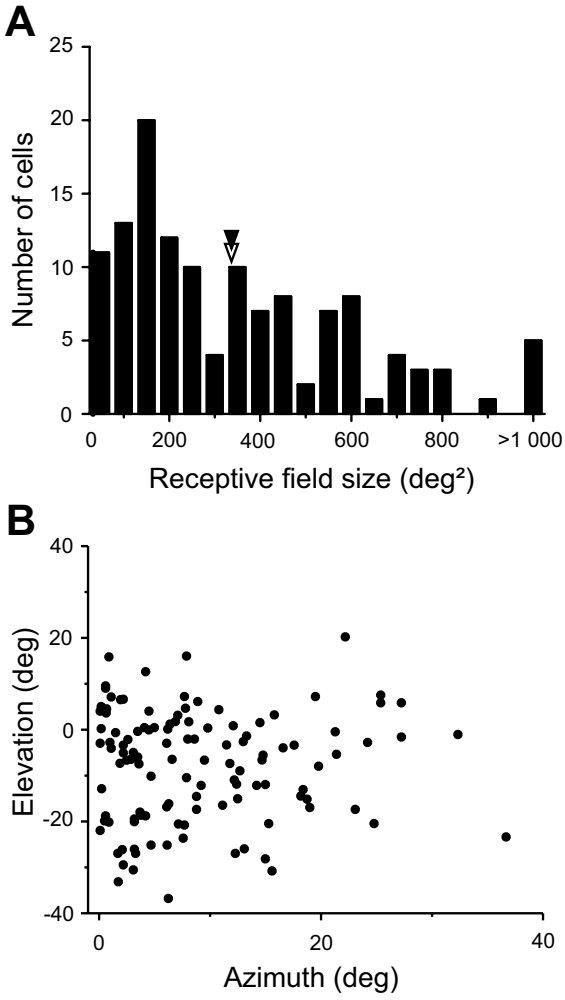

Fig. 2. Receptive field characteristics. A: Distribution of receptive field size of AMLS neurons. The mean (354±276°²) and median (348°²) are represented by the filled and empty triangles respectively. B: Position of receptive field centers in relation to the area centralis. Receptive field centers were determined as the geometrical center of hand plotted areas that evoked a visual response. The majority of receptive field centers were in the lower visual field and most were within 20° of the area centralis along both horizontal and vertical meridians.

direction bandwidths is shown in panel C. The mean±S.D. was 32±17°, ranging from 9.6 to 96.8°. Although a broad range of DI values was found, from 0.02 to 1.8 (mean 0.73±0.35), most neurons (54 of 73; 74%) were direction selective (panel D). Neither bandwidth (r=0.16; P=0.12) nor DI (r=0.12, P=0.33) was observed to vary along the antero-posterior axis of AMLS cortex. No preferred direction was represented significantly more often (χ^2=8.34; P>0.10) than would be expected of a homogeneous distribution. AMLS neurons retained their direction selectivity even at the lowest spatial frequencies tested (generally 0.01 c/°).

Visual noise. Direction selectivity of AMLS cells was further assessed by presenting visual noise to a sample of neurons. Twenty-five out of 37 neurons responded to the visual noise and 19 of those were direction selective (DI>0.5). The remaining 12 neurons could not be driven by this stimulus. A typical direction-tuning curve for visual noise pattern is presented in panel A of Fig. 4 (filled symbols). This cell was direction selective and exhibited relatively broad direction tuning (bandwidth of 27.1°). Of note is the fact that the preferred direction for visual noise did not match that observed for gratings, and that the cell's direction selectivity differed between the two stimuli (see below). None of the neurons showed a bimodal direction-tuning curve similar to that observed by Hammond and Reck (1980) in area 17.

Overall, most AMLS neurons were more broadly tuned for visual noise than for grating direction. Panel B of Fig. 4 shows the relationship between bandwidth values on a cell by cell basis: clearly most data points rest above the line of perfect regression. This difference was not present (t=1.448; P=0.15) when the data were pooled across cells. The mean visual noise bandwidth was 38.1±17.6° (ranging between 17.4 and 89°) as compared with 32±17° for gratings. The DI of the sample ranged from 0.07 to 1.43 with a mean of 0.72±0.36. As shown in the example of panel A, the strength of direction selectivity and the preferred direction could considerably differ according to the stimulus. There was no clear relationship between the direction selectivity indices of AMLS neurons computed from grating and visual noise responses. This is clearly illustrated in panel C of Fig. 4. Data points are scattered on each side of the perfect regression line and a large proportion of cells were direction-selective for only one of the two stimuli (upper-left and lower-right quadrants). A comparison of preferred directions for gratings and visual noise revealed that for 12 of 19 neurons, the optimal direction differed by more than 30° (Fig. 5A).

RDKs. Global motion sensitivity of AMLS neurons was first studied by comparing direction selectivity of a subset of 24 and 22 neurons to simple and complex RDK stimuli, respectively. A representative example of an RDK direction-selective cell is shown in panels A–C of Fig. 6. For comparison purposes, panel A depicts the responses to a drifting grating. Panels B and C show that the unit responded equally well to simple and complex RDKs, indicating that it is global motion sensitive. Selectivity to both simple and complex RDKs was present among most AMLS neurons tested (18 of 22 units, 82% for complex RDKs; against 19 of 24, 79% for simple RDKs). Overall, the mean bandwidth for direction computed from simple and complex RDKs (42±15°, range 15–69.1°, and 52±27°, range 12.4–94.2°, respectively) was significantly greater for simple (t=2.037; P=0.044) and complex RDKs (t=3.399; P<0.001) than that computed from gratings (see the distribution in Fig. 7A). Tuning for AMLS cells was not broader for complex than for simple RDKs (t=1.159; P=0.258).

Two other observations can be made. First, as in Fig. 6A–C, most cells remained direction selective for all three stimuli. This is illustrated in panel B of Fig. 7 in which the distribution of DIs for both types of RDKs is plotted as a

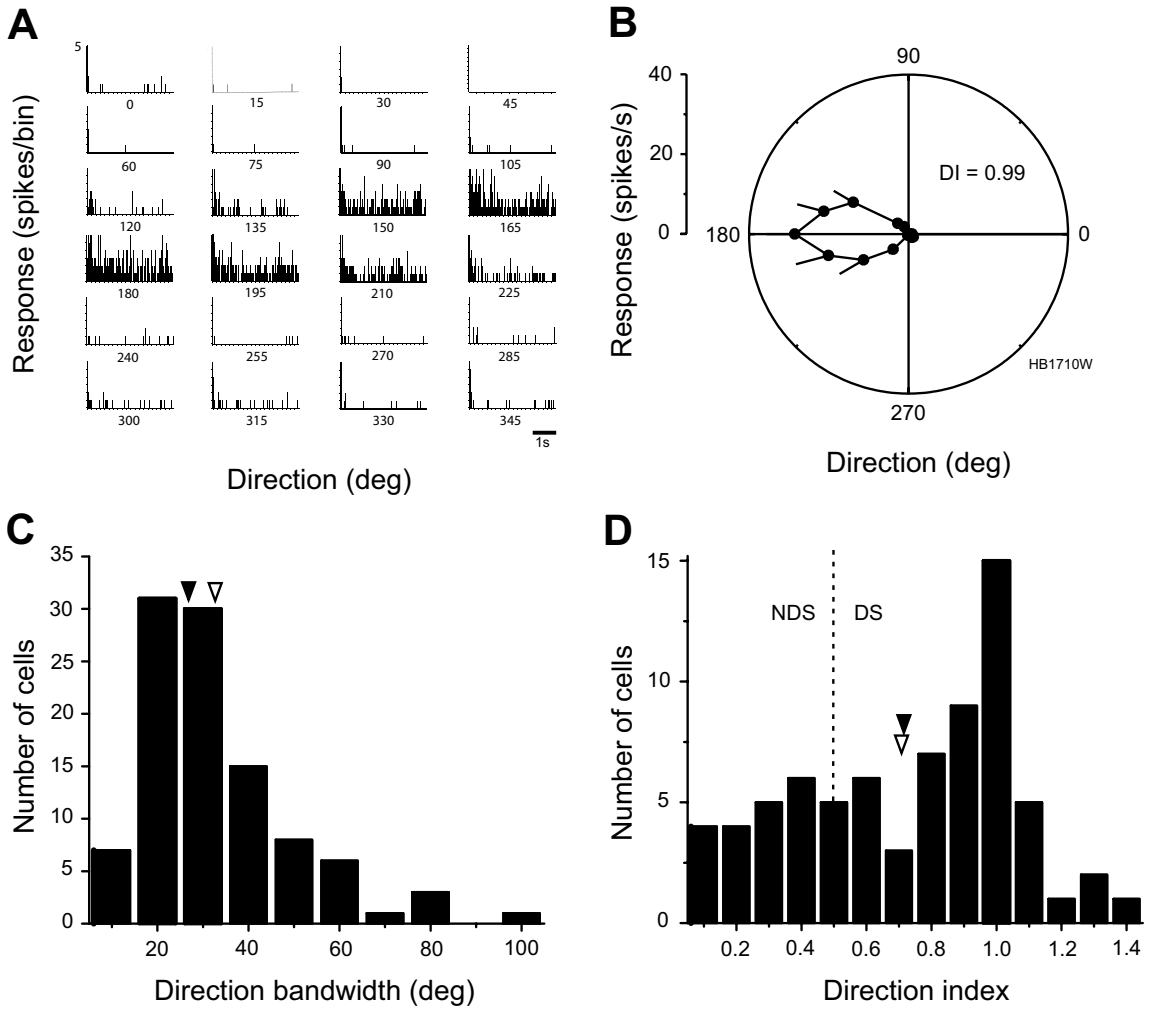

Fig. 3. Direction selectivity to gratings. A: A representative example of the response profile to a drifting sine wave grating (0.02 c/°; 7 Hz). Discharge rate is shown in PSTH form, generated from four repetitions each lasting 4 s. B: Direction tuning curve of the same cell presented in A. Responses are shown as mean±S.E.M. Spontaneous activity is too low to be seen (0.62 spikes/s). C: Distribution of direction bandwidths (median of 38°). D: Distribution of DI. The dashed line represents the limit between non-direction (NDS) and direction selective (DS) neurons. Mean and median values are represented as in Fig. 2.

function of grating DIs. Most data points are placed in the upper-right quadrant (direction-selective cells) while a subset lie in the upper-left quadrant. In the latter case, neurons were more direction selective for RDKs than for grating stimuli. Mean DIs were not significantly different (t=0.638; P=0.527) for simple (0.93±0.21; range: 0.52–1.26) and complex RDKs (1.00±0.48; range: 0.35–2.23). The DI values obtained with both simple (t=2.316; P=0.023) and complex RDKs (t=2.778; P=0.007) were significantly different from that observed with gratings (0.93±0.21). The second observation is that preferred directions varied little among the three stimuli used (panels B and C, Fig. 5), and this is especially true between simple and complex RDKs (panel C). As in the case of visual noise, no neurons were observed to be selective to more than one direction of motion. The preferred direction exhibited for RDKs did not vary over velocities ranging from 1 to 500°/s.

As a general rule, simple RDK direction-selective neurons were also direction selective for complex RDKs. Only one of 16 neurons tested with both stimuli was not responsive to complex RDKs. More interesting perhaps, is the fact that a few AMLS neurons exhibited direction selectivity to complex but not to simple motion RDKs. For example, the neuron presented in panel D of Fig. 6 responded to all directions of motion of a simple RDK (empty symbols), but exhibited a broad (87.3°) yet clear direction selective tuning curve to complex motion RDKs (filled symbols). Among our sample of neurons, three were uniquely selective to complex motion RDKs.

Optic flow fields. Radial optic flow sensitivity was tested for 20 neurons in AMLS cortex to further reveal global motion sensitivity. Optic flow elicited a response in 13 of the 20 neurons tested. Of these, nine were selective to the direction of motion of the optic flow stimulus, five neurons preferred contracting motion, and four expanding motion. The neurons in Fig. 8 are representative examples of contracting and expanding mo-

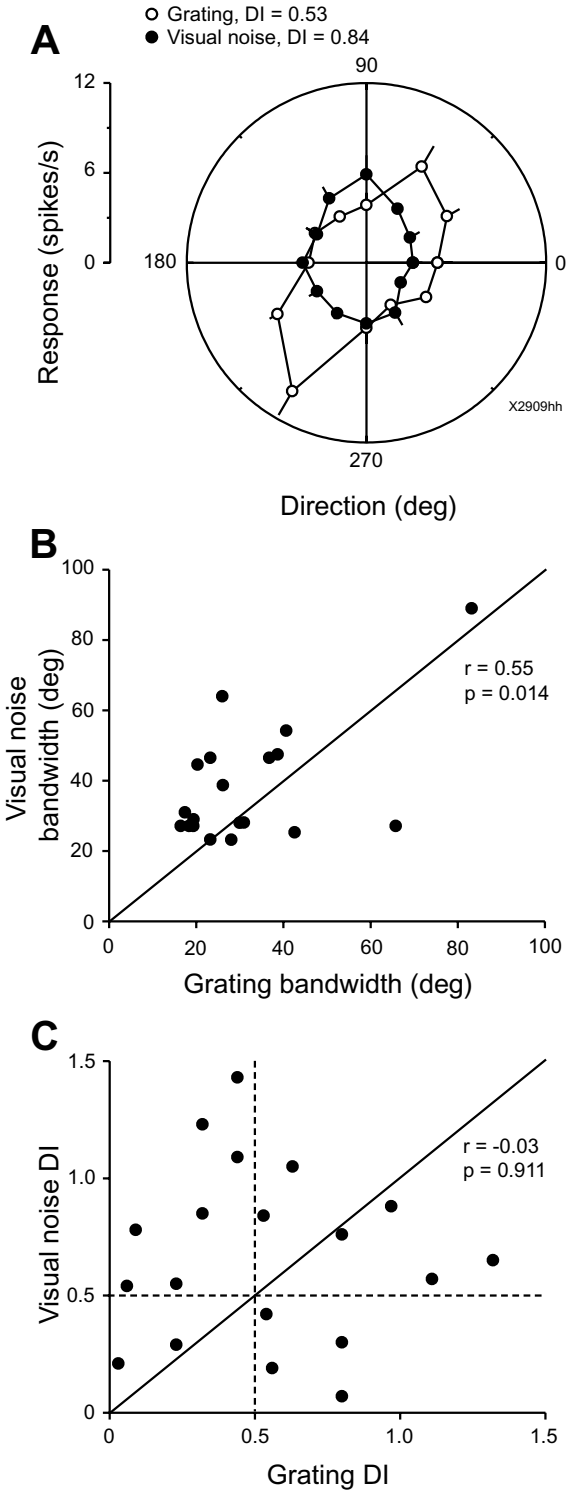

Fig. 4. Direction selectivity to visual noise. A: Neuronal response to different directions of motion of a noise pattern (filled symbols) and a sine wave grating (empty symbols). Responses are shown as mean±S.E.M. B: Correlation between visual noise and grating bandwidths. C: Correlation between DIs for visual noise and drifting gratings. The dashed lines represent the limit between direction and non-direction selective neurons as per Fig. 3. Diagonals in panels B and C are lines of perfect regression. Correlation coefficients are given.

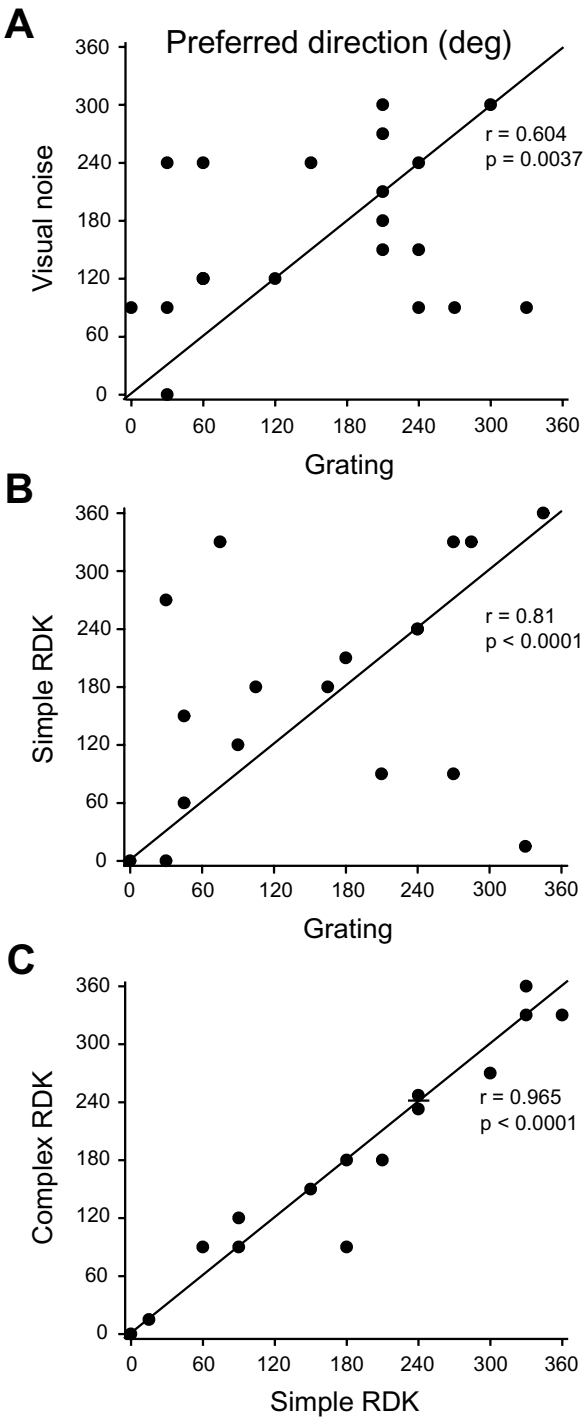

Fig. 5. Relationship between the preferred directions for (A) sine wave gratings and visual noise patterns (B) gratings and simple RDKs, and (C) simple and complex RDKs. Note that a few data points could be misinterpreted. For example, the cell in Panel B with a preferred direction of 330° for gratings and 15° for simple RDKs could be interpreted as having preferred directions that differ by 315°. In fact the cell's preferred directions differed by only 45° due to the circular nature of direction. This fact was taken into account when calculating the correlation coefficients in A–C. In C, superimposed data points have been symmetrically shifted about an axis represented by a short horizontal line. Conventions are as in Fig. 4.

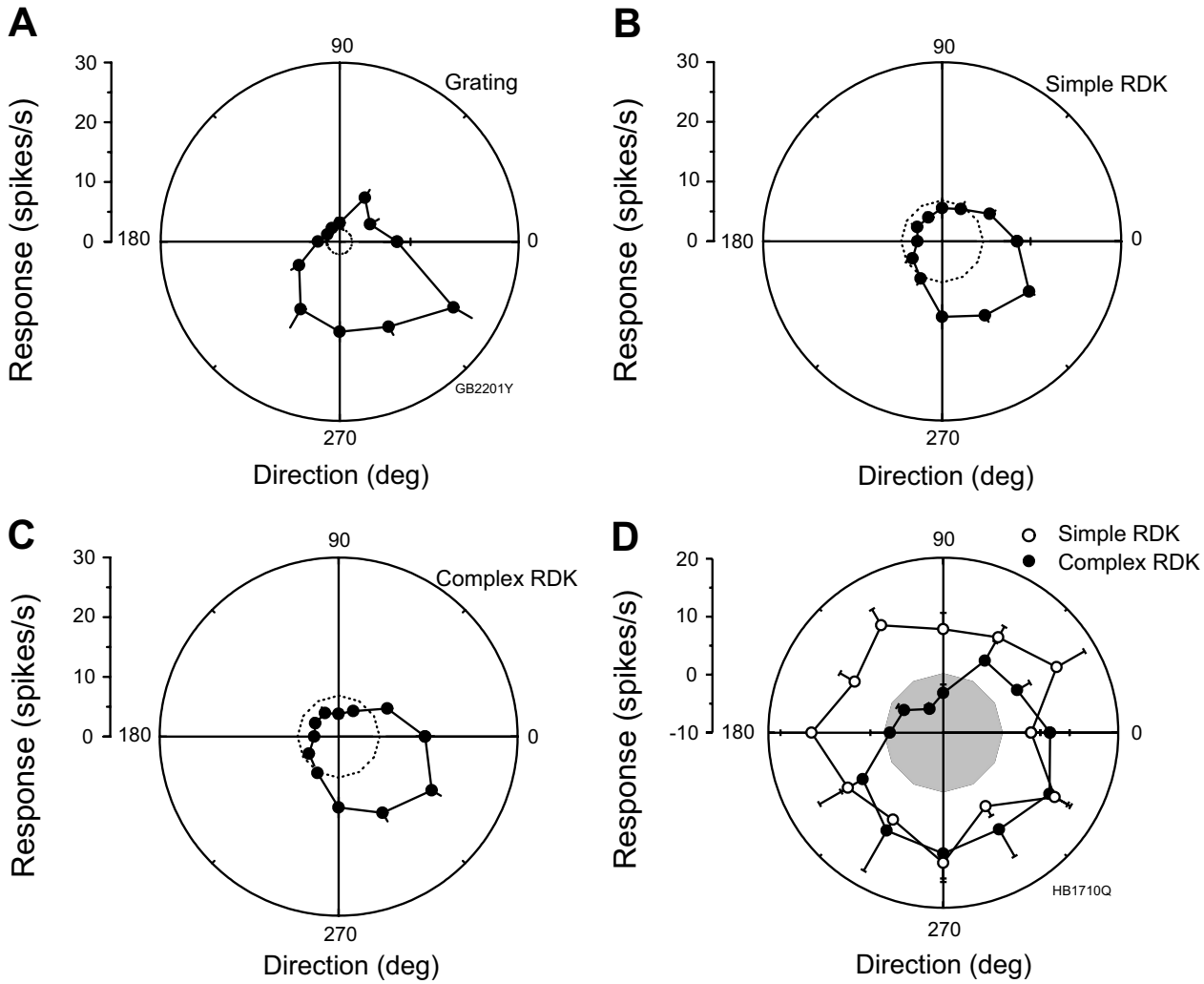

Fig. 6. Direction selectivity to RDKs: Polar plots of the response of an AMLS neuron to a drifting sine wave grating (A), a simple RDK (B) and a complex RDK (C) are presented. Responses are shown as mean±S.E.M. Dotted lines represent spontaneous activity levels. D: Example of a cell that was direction selective to complex RDKs (filled circles), but exhibited no direction selectivity to simple RDKs (empty circles). Spontaneous activity has been subtracted from the mean response level: data points within the shaded area represent cell discharges below spontaneous activity levels.

tion selective cells. In panel A, the unit responded vigorously to contracting motion. Response amplitude for expanding motion and spontaneous activity was low and almost indistinguishable. In panel B, the unit exhibited a relatively high baseline level and was clearly selective for stimulus expansion.

Axial direction (see Experimental Procedures) was studied for 92 AMLS neurons. Fig. 8C shows that there was no clear preference for centrifugal (distribution around 0°) or centripetal directions (around 180°; $\chi^2=14.8$; $P>0.10$).

Plaid patterns. Direction selectivity to plaid patterns was assessed among a sample of 38 neurons. Eight cells were found to have a PM selective response similar to that presented in panel A of Fig. 9. Note that the PM selective cell was more broadly tuned for drifting gratings than the CM selective cell (compare open-symbol tuning curves in panels A and B). This observation persisted when all cells were pooled and mean bandwidths computed (51±22°, and 31±16° for PM and CM selective neurons, respectively). The result of statistical analyses of plaid response profiles for the entire sample is presented in panels C and D. Panel C shows the original method of analysis: in that case, five and 13 neurons were classified as pattern and CM selective, respectively. When partial correlation coefficients were transformed to Z scores (panel D), a larger subpopulation (21%) of AMLS neurons was found capable of coding for the veridical direction of a plaid pattern. Note that CM response profiles were also present (68%, $n=26$) and represented the largest subset of the sample. A smaller group of neurons (11%, $n=4$) had a response profile that could not be unequivocally classified and were therefore considered as direction selective unclassified. No bias toward larger receptive fields was found to exist among PM selective neurons; this could not be verified statistically due to sample size.

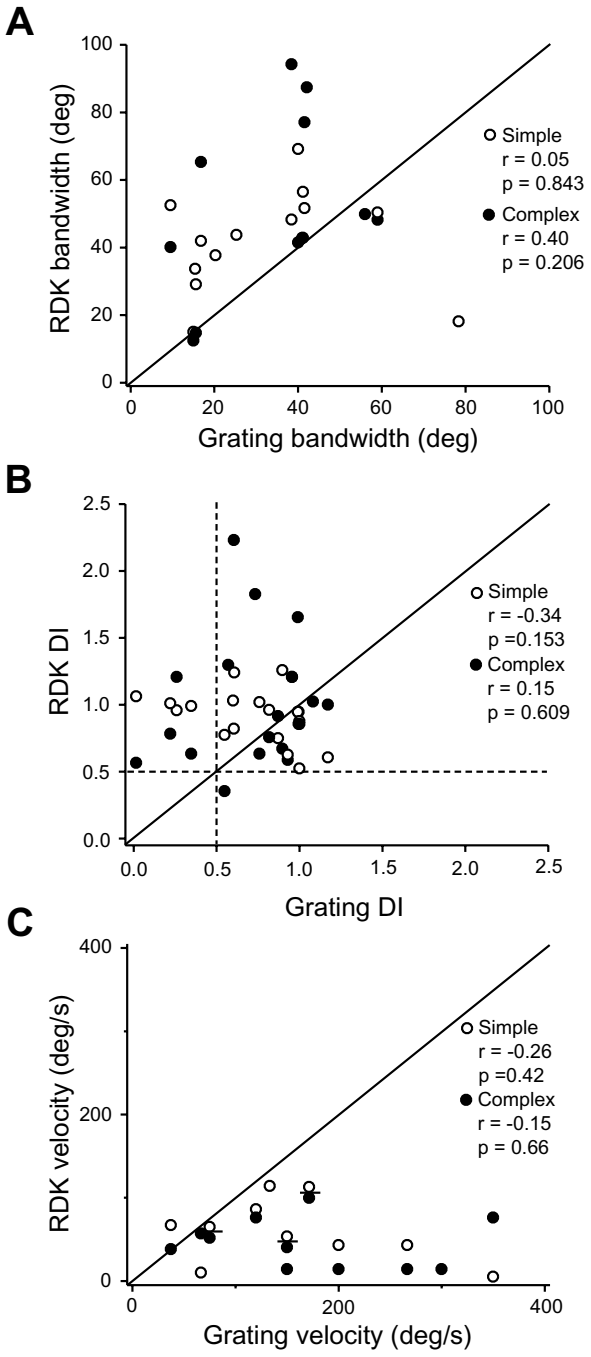

Fig. 7. Relationship between grating and RDK responses. A: Plotted is simple (empty symbols) and complex (filled symbols) RDK bandwidth as a function of sine wave grating bandwidth. B: Correlation between DIs for simple and complex RDKs and gratings. The dashed lines represent the limit between direction and non-direction selective neurons as per Fig. 3. C: Comparison of optimal velocities for sine wave gratings with that for simple and complex RDKs. The optimal velocity for one type of stimulus is clearly not predictive of the other. Superimposed data points have been symmetrically shifted about an axis represented by a short horizontal line. Diagonals represent the line of perfect regression. Correlation coefficients are given.

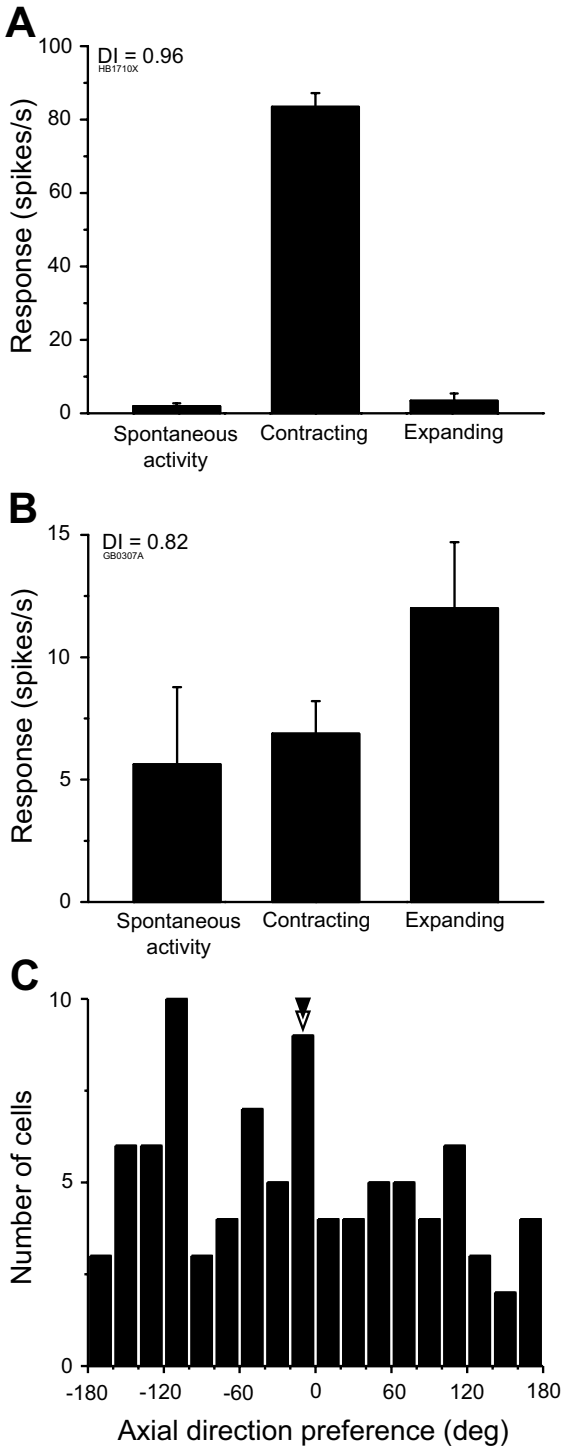

Fig. 8. Direction selectivity to optic flow fields. A and B: Examples of AMLS neurons that were contracting and expanding selective to an optic flow field respectively. The DI is given for both neurons. Responses are shown as mean±S.E.M. C: Distribution of axial direction preference for gratings. Mean and median are represented as per previous figures.

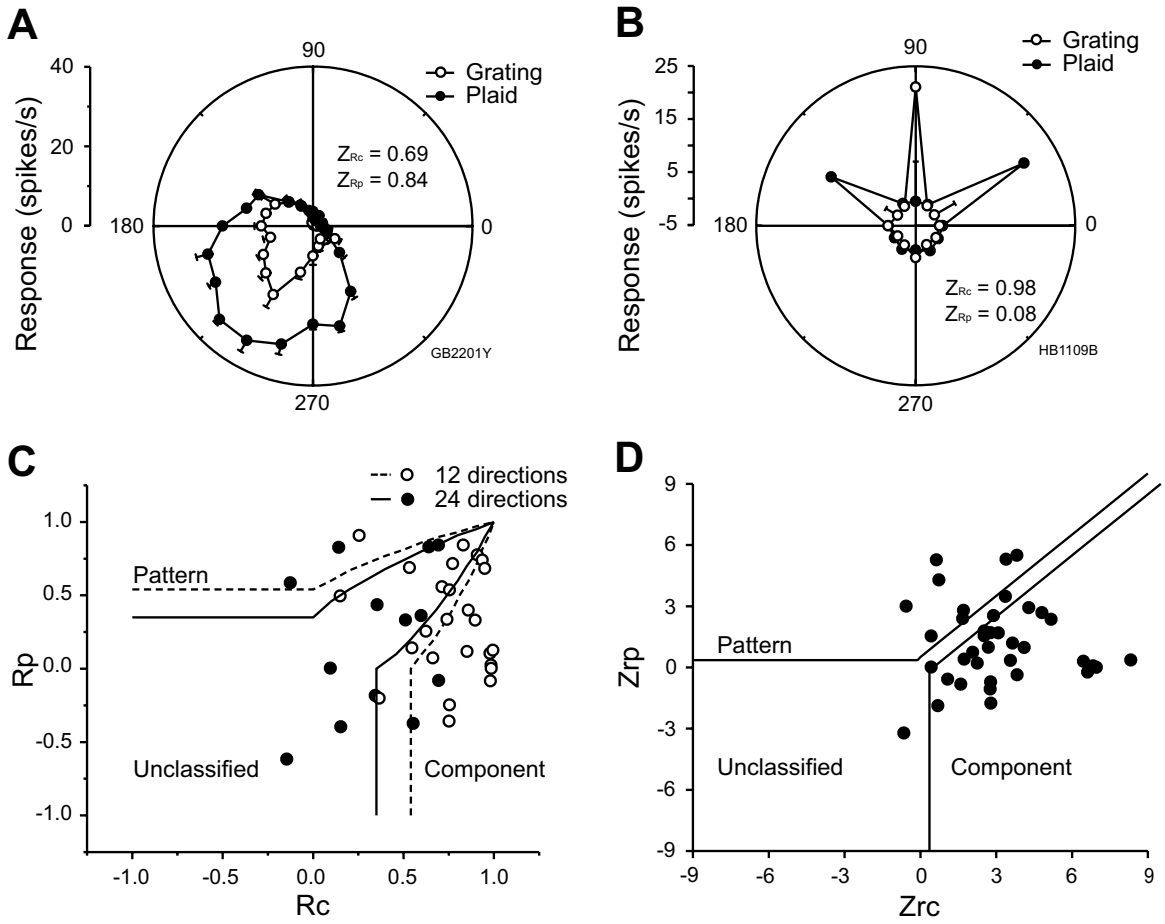

Fig. 9. Direction selectivity to plaid patterns. A and B: Response profiles of pattern (A) and component (B) motion selective cells (filled symbols). Responses to sine wave gratings (empty symbols) are presented. Spontaneous activity was omitted for clarity (3.25 and 1.31 spikes/s, respectively). C: Scatter plot in which the partial correlation coefficients for component (R_C) and pattern (R_P) motion are plotted against each other, using the conventional method of analysis. The data space is divided into three statistical regions. Cells falling in the upper left and lower right areas are respectively pattern- and component-motion selective. The points lying in between represent unclassified direction-selective cells. Responses were computed from tests performed at 12 (dashed lines and empty symbols) and 24 (full lines and filled symbols) directions. D: Scatter plot in which the corresponding Z values for R_C and R_P are plotted. The *z* score transformation allows the merging of all data, and yields a reduction of the unclassified statistical area.

Velocity selectivity

Values for different stimuli were compared to determine if optimal velocities were stimulus dependent. The mean optimal velocity for gratings (201±192°/s; computed from optimal spatial and temporal frequency values, see below) was significantly different from the mean optimal speed for simple (66±39°/s; range: 5–143°/s; t=2.59; P=0.013) and complex motion RDKs (57±35°/s; range: 14–119°/s; t=2.564; P=0.014). These differences were supported by comparing velocities for each neuron individually (Fig. 7C). There was no significant difference in optimal velocity between both types of RDKs (t=0.615; P=0.545). The mean optimal velocity for visual noise patterns (44.36±30.18°/s, range: 1 and 107°/s) was significantly different from that of gratings (t=3.62; P<0.001), but not significantly different from mean velocities computed for simple (t=1.86; P=0.072) and complex RDKs (t=1.12; P=0.274).

Spatial and temporal contrast sensitivity

Receptive fields in AMLS cortex were optimally driven by low spatial frequency gratings. Most cells tested (33 of 42) were band-pass tuned as that shown in panel A of Fig. 10 (open symbols). A second subset of cells, eight of 42, exhibited a low-pass tuning profile (filled symbols in panel A). The remaining neuron exhibited no clear preference for spatial frequency. Panel B shows the distribution of optimal spatial frequency values: they ranged from 0.01 to 0.3 c/° and the mean was 0.03±0.02 c/° (median of 0.02 c/°). Tuning functions were broad with a mean bandwidth of 1.63±0.36 octaves (panel C) and ranged from 1.1 to 2.5. Among band-pass tuned cells, the mean low cutoff was 0.04±0.04 c/° and the high cutoff value was 0.10±0.12 c/°. The high cutoff value for low-pass cells was 0.06±0.06 c/°. Optimal spatial frequency and tuning width did not vary along the antero-posterior axis of the

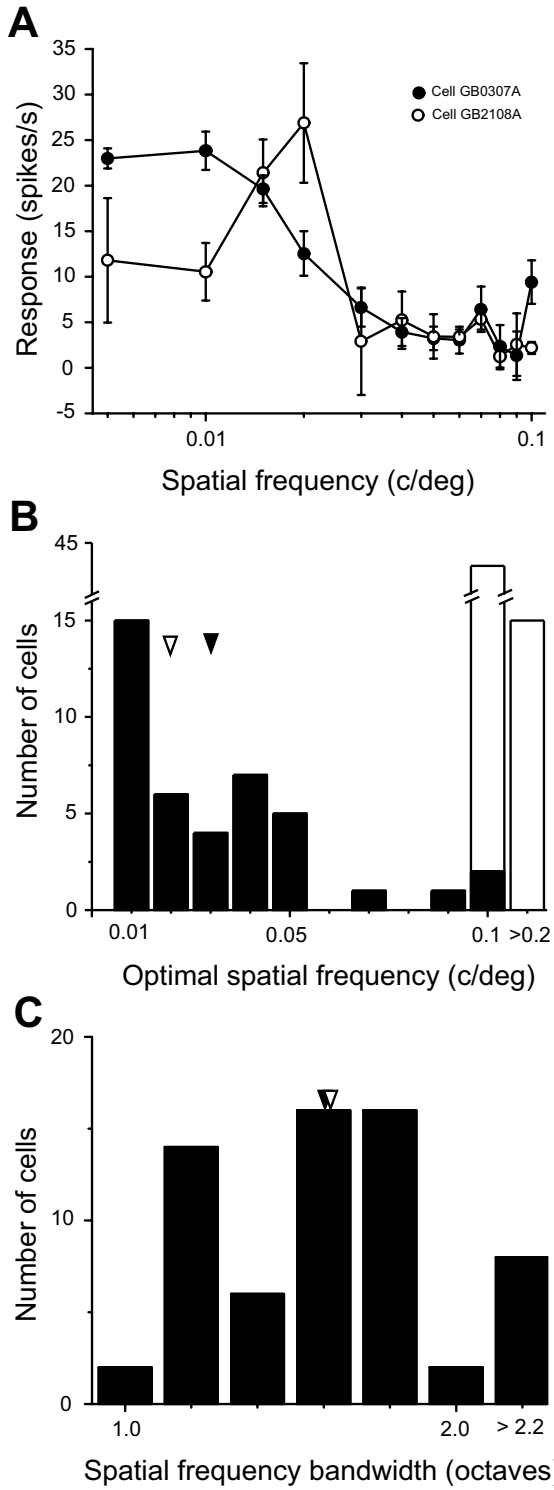

Fig. 10. Spatial contrast sensitivity. A: Two representative spatial frequency tuning functions. A subset of neurons sampled exhibited low pass tuning (filled symbols); however the majority of neurons had a band pass response profile (open symbols). Responses are shown as mean±S.E.M. B: Distribution of optimal spatial frequencies. Values obtained with the VS software (empty bars) are presented for comparison purposes with previous studies (see Experimental Procedures). C: Distribution of spatial frequency bandwidth. Mean and median values are represented as in previous figures.

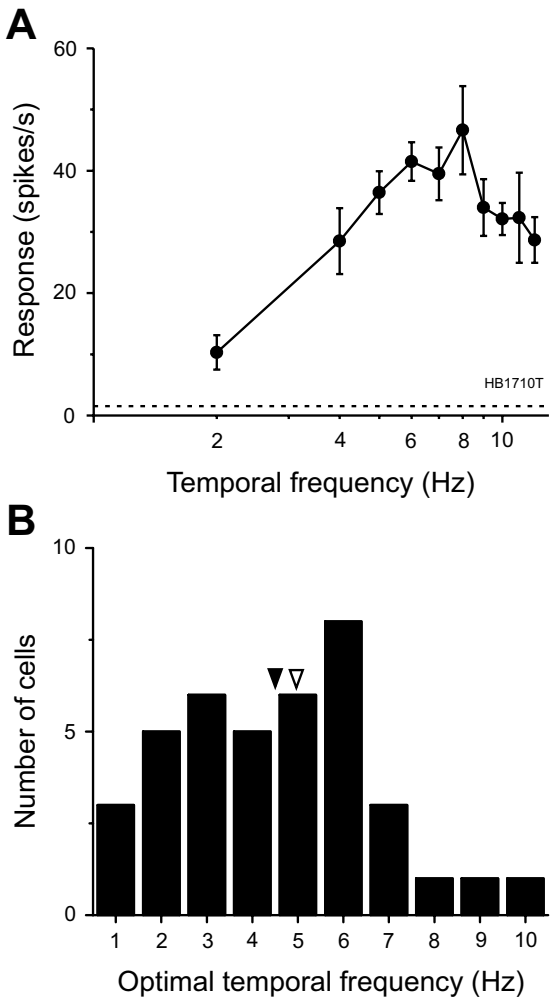

Fig. 11. Temporal contrast sensitivity. A: Cell response as a function of grating temporal frequency. Responses are shown as mean±S.E.M. B: Distribution of optimal temporal frequencies in AMLS cortex. Mean and median are represented as per previous figures.

AMLS cortex ($r=0.09$, $P=0.37$; $r=-0.55$, $P=0.62$, respectively). A significant negative correlation ($r=-0.40$; $P=0.03$) was found between optimal spatial frequency and receptive field eccentricity. Surprisingly, preferred spatial frequency was not correlated with receptive field size ($r=-0.19$; $P=0.07$), despite a significant correlation between receptive field size and eccentricity ($r=0.26$; $P=0.003$).

Temporal frequency selectivity was assessed for a subset of 50 neurons. Of these, 41 showed a preference for a particular temporal frequency and nine neurons were not selective for temporal frequency. These non-selective neurons responded above baseline to gratings, but response amplitude did not vary as a function of the stimulus temporal frequency. Of the 41 cells exhibiting a preferred temporal frequency, 39 were similar to the neuron illustrated in Fig. 11A. A bandwidth could not be calculated for these cells, as response amplitude did not taper off at the

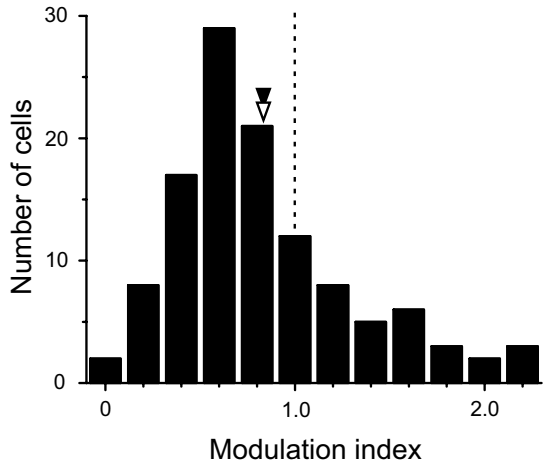

Fig. 12. Response profile. Distribution of modulation indices in AMLS cortex. The dashed line represents the limit between cells that exhibited a modulation of their discharges (MI>1) and those that did not (MI<1). Mean and median values are presented as per previous figures.

highest temporal frequencies tested. Only two neurons showed a low-pass response profile; the lowest temporal frequency tested with these neurons was 1 Hz (rather than 0.5 Hz as with other neurons). The optimal temporal frequency observed in AMLS cortex ranged between one and 10 Hz, with a mean of 4.5±2.2 Hz (Fig. 11B). Optimal temporal frequency was not observed to systematically vary with the antero-posterior position of the electrode ($r=-0.10$, $P=0.56$), nor with receptive field eccentricity ($r=0.19$; $P=0.32$).

Response profile

As for the cell presented in panel A of Fig. 3, most AMLS neurons responded to sine wave gratings with no strong modulation of their discharges. An MI was computed for a subset of neurons ($n=34$) for which both clear spatial and temporal frequency tuning functions were observed. This mean MI was not significantly different ($t=0.3$; $P=0.77$) from that of all neurons ($n=116$, including those driven by the VS system) for which an MI was calculated (e.g. neurons that responded equally well to all temporal frequencies, were low-pass tuned for spatial frequency, etc.). Therefore, the MI for the entire sample is presented here. Fig. 12 shows that most cells (86/116) had a MI under 1.0, with a mean of 0.84±0.49. Note that the distribution is skewed to the left, which is indicative of neurons that do not have segregated ON and OFF regions (complex-like receptive fields), which agrees with the qualitative assessment of receptive field structure reported above. Response modulation did not vary along the antero-posterior axis of AMLS cortex ($r=-0.15$; $P=0.11$).

DISCUSSION

General observations

Visual neurons in AMLS cortex are generally characterized by large receptive fields that are centered close to or below the area centralis. Most are highly direction selective and are broadly tuned to a number of different stimuli. Of particular interest is the fact that neurons in AMLS cortex are capable of signaling the PM of a plaid and the direction of complex motion RDKs. These findings suggest that AMLS cortex may represent a higher order cortical region that is part of a network of visual areas that are involved in the processing and integration of visual motion cues.

Simple motion direction selectivity

The present study demonstrates that neurons in AMLS cortex are highly direction selective not only to drifting sine wave gratings, but also to visual noise and simple motion RDKs. Differences between the responses to these stimuli raise questions as to the afferent connections that give rise to direction selectivity in AMLS cortex. Many cells (12/19) did not share the same optimal direction for sine wave gratings and visual noise patterns. Average direction indices, bandwidths, and optimal velocity were also stimulus dependent. Differences in optimal directions have previously been noted in PMLS cortex (Merabet et al., 2000). It may be suggested that this discrepancy is due to the phenomenon reported by Hammond and Reck (1980), where preferred direction varies as a function of speed. This explanation is not likely, as some cells were tested with RDKs covering a range of 1–500°/s and the preferred direction remained constant over this range of values (not shown). These differences may be attributable to the large discrepancy in spatial scale of the stimuli presented. Element size for visual noise was 0.13°, each dot in the RDK pattern covered 1°, and a single cycle of a sine wave grating presented at the mean optimal spatial frequency covered 33.3° (or 50° in the case of the median and 100° for the mode).

Complex motion direction selectivity

Neurons in AMLS cortex were direction selective to complex motion stimuli, such as plaid patterns and complex RDKs. Neurons in AMLS cortex are involved therefore, in plaid-defined complex motion processing. Despite the small number of neurons, we believe that this is of fundamental importance given that AMLS cortex is the only visual cortical area in the cat, other than the AEV (Scannell et al., 1996), that has a population of PM selective cells. Also of interest is the fact that the largest subset of the sample in the present study was CM selective, thus establishing AMLS cortex as the only cortical area so far, in the cat, that has both CM and PM selective neurons.

Plaid PM selectivity suggests a possible functional hierarchy of visual areas within cat cortex that is in accord with the scheme of Hilgetag et al. (2000), in which AMLS cortex is situated between PMLS and AEV cortex. Plaid PM selective neurons are not present in PMLS cortex (Gizzi et al., 1981; Movshon et al., 1986; Merabet et al., 1998; Villeneuve and Casanova, 2001); they are present in intermediate proportions in AMLS cortex (the present study), and there is a large population of such cells in the AEV (Scannell et al., 1996). The hierarchical scheme is further supported by previous neuroanatomical studies

which have shown that AMLS cortex receives afferents from PMLS (Symonds and Rosenquist, 1984a,b), whereas AMLS cortex neurons project to AEV cortex (Miceli et al., 1985; Olson and Graybiel, 1987). Furthermore, AMLS cortex does not receive strong projections from lower visual centers such as the primary visual cortex (Sherk, 1986; Shipp and Grant, 1991), whereas PMLS cortex does. It should be noted however, that this proposed hierarchy does not preclude that other cortical and subcortical areas may play a role in the transfer of information between these regions.

One can speculate as to the origin of the PM selectivity. PM selective cells in AMLS cortex may be attributable to afferent signals from higher-order subcortical (LP-pulvinar) and cortical (AEV) areas known to be PM selective (Scannell et al., 1996; Merabet et al., 1998; Casanova et al., 2001; Dumbrava et al., 2001). Alternatively, in the line of thinking of Scannell et al. (1996), it is possible that AMLS cortex represents the first stage of intrinsic cortical computations that permit PM selective neuronal responses. In support of this assumption, Merabet et al. (1998; see also Casanova et al., 2001) have demonstrated that a lesion of the AEV is insufficient to eliminate PM responses in the LP-pulvinar. This suggests that another cortical region may be, at least partially, responsible for the PM selective responses seen in the LP-pulvinar. Our results indicate that the AMLS could be such a region.

Complex RDK direction selectivity reinforces the higher-order nature of visual motion processing in AMLS cortex. Furthermore, a subset of these neurons was not simple RDK selective. Were AMLS cortex inheriting its motion selectivity from lower visual areas, one would expect neurons in this area to be simple RDK direction selective. The presence of complex but not simple RDK direction selectivity suggests that neurons in AMLS are involved in an intrinsic higher-order analysis of visual motion cues.

Comparison with PMLS cortex

Both AMLS and PMLS cortices lie along the medial bank of the lateral suprasylvian sulcus and share a large part of their connectivity patterns (Symonds et al., 1981; Updyke, 1981; Raczkowski and Rosenquist, 1983; Symonds and Rosenquist, 1984a,b; Olson and Graybiel, 1987; Norita et al., 1996). One may wonder if they actually represent two distinct areas as has been reported previously in the literature based on electrophysiological data (Palmer et al., 1978; Toyama et al., 1990), differences in myeloarchitecture (Sanides and Hoffmann, 1967), differential protein expression (van der Gucht et al., 2001), different levels of 2-deoxyglucose uptake (Vanduffel et al., 1997), and differential projection patterns from area 17 (Sherk, 1986; Grant and Shipp, 1991). These previous studies in conjunction with the presence of PM selective cells in AMLS cortex, but not in PMLS cortex (Gizzi et al., 1981; Movshon et al., 1986; Merabet et al., 1998; Villeneuve and Casanova, 2001) suggests that they are indeed two separate computational units. These physiological and anatomical distinctions prompted us to quantitatively compare data gathered for these two regions.

For the following comparisons, unpublished PMLS data from our laboratory were employed (for details on other data for PMLS cortex see Spear and Baumann, 1975; Camarda and Rizzolatti, 1976; Di Stefano et al., 1985; Morrone et al., 1986; Movshon et al., 1986; Zumbroich et al., 1986; Zumbroich and Blakemore, 1987; Gizzi et al., 1990; Kim et al., 1997; Merabet et al., 1998; Villeneuve and Casanova, 2001). Only a short list of important differences is given. Mean optimal spatial frequency in AMLS was lower than in PMLS cortex ($t=-4.541$; $P<0.001$), whereas the opposite was true for mean optimal temporal frequency ($t=2.362$; $P<0.021$). The mean optimal velocity for simple RDKs in PMLS (30 ± 17°/s) cortex is statistically below ($t=4.446$; $P=<0.001$) that for neurons in AMLS cortex (66 ± 39). In PMLS cortex, approximately two thirds of the population is selective to the simulation of expanding motion (Brosseau-Lachaine et al., 2001), whereas our preliminary data indicate that equal proportions of neurons in AMLS cortex are selective to contracting and expanding motion. These statistically significant differences strongly support the previous evidence that AMLS and PMLS cortex do not represent one large functional unit, but rather, are two distinct regions, with similar response properties within the same visual pathway.

General conclusions

Based on our data and on neuroanatomical considerations (Symonds and Rosenquist, 1984a,b; Miceli et al., 1985; Olson and Graybiel, 1987; Hilgetag and Grant, 2001), we propose that AMLS cortex is situated between PMLS and AEV cortices in a functional hierarchy of visual areas. This functional hierarchy suggests that AMLS cortex is part of a network of regions that is responsible for the processing of visual motion cues. Despite the known selectivity for motion-in-depth and higher order motion stimuli, the behavioral significance of the signals emanating from neurons in AMLS cortex remains to be determined.

Acknowledgements—This work was supported by a CIHR grant to C.C. Part of the salary of C.C. was supported by the FRSQ. B.G.O. was supported in part by a réseau FRSQ en santé de la vision studentship. We thank D. Boire for his aid in the statistical analysis of plaid pattern response profiles and M. Villeneuve for providing unpublished data concerning response properties in PMLS cortex. We also thank M. von Grünau and C. Baker for helpful comments on previous versions of this manuscript, and J. A. Movshon for information and formulas related to the novel method of analysis of plaid pattern responses.

REFERENCES

Bishop PO, Kozak W, Vakkur GJ (1962) Some quantitative aspects of the cat's eye: axis and plane of reference, visual field co-ordinates and optics. J Physiol 163:466–502.

Brosseau-Lachaine O, Faubert J, Casanova C (2001) Functional subregions for optic flow processing in the posteromedial lateral suprasylvian cortex of the cat. Cereb Cortex 11:989–1001.

Camarda R, Rizzolatti G (1976) Visual receptive fields in the lateral suprasylvian area (Clare-Bishop area) of the cat. Brain Res 101: 427–443.

Casanova C, Merabet L, Desautels A, Minville K (2001) Higher-order motion processing in the pulvinar. Prog Brain Res 134:71–82.

Casanova C, Savard T (1996) Responses to moving texture patterns of cells in the striate-recipient zone of the cat's lateral posterior-pulvinar complex. Neuroscience 70:439–447.

Casanova C, Savard T, Nordmann S, Molotchnikoff S, Minville K (1995) Comparison of the responses to moving texture patterns of simple and complex cells in cat's area 17. J Neurophysiol 73:1271–1286.

Di Stefano M, Morrone MC, Burr DC (1985) Visual acuity of neurones in the cat lateral suprasylvian cortex. Brain Res 331:382–385.

Dreher B, Wang C, Turlejski KJ, Burke W (1996) Areas PMLS and 21a of cat visual cortex: two functionally distinct areas. Cereb Cortex 6:585–589.

Dumbrava D, Faubert J, Casanova C (2001) Global motion integration in the cat's lateral posterior-pulvinar complex. Eur J Neuro 13: 2218–2226.

Gibson JJ (1950) The stimulus variables for visual depth and distance: the active observer. In: The perception of the visual world (Carmichael L, Ed), pp 117–144. Boston, MA: Houghton Mifflin.

Gizzi MS, Katz E, Movshon JA (1981) Orientation selectivity in the cat's lateral suprasylvian visual cortex. Inv Ophthalmol Vis Sci 149 (suppl. 20):149.

Gizzi MS, Katz E, Movshon JA (1990) Spatial and temporal analysis by neurons in the representation of the central visual field in the cat's lateral suprasylvian visual cortex. Vis Neurol 5:463–468.

Grant S, Shipp S (1991) Visuotopic organization of the lateral suprasylvian area and of an adjacent area of the ectosylvian gyrus of cat cortex: a physiological and connectional study. Vis Neurol 6:315–338.

Hammond P, Reck J (1980) Influence of velocity on directional tuning of complex cells in cat striate cortex for texture motion. Neurosci Lett 19:309–314.

Hilgetag CC, Grant S (2001) Uniformity and specificity of long-range corticocortical connections un the visual cortex of the cat. Neurocomputing 38-40:667–673.

Hilgetag CC, O'Neill MA, Young MP (2000) Hierarchical organization of macaque and cat cortical sensory systems explored with a novel network processor. Phil Trans R Soc Lond B 355:71–89.

Kawamura K, Naito J (1980) Corticocortical neurons projecting to the medial and lateral banks of the middle suprasylvian sulcus in the cat: an experimental study with the horseradish peroxidase method. J Comp Neurol 193:1009–1022.

Kim J-N, Mulligan K, Sherk H (1997) Simulated optic flow and extrastriate cortex: I. Optic flow versus texture. J Neurophysiol 77:554–561.

Lomber SG (2001) Behavioral cartography of visual functions in cat parietal cortex: areal and laminar dissociations. Prog Brain Res 134:265–284.

Majaj N, Carandini M, Smith MA, Movshon JA (1999) Local integration of features for the computation of pattern direction by neurons in macaque area MT. Soc Neurosci Abstr 25:674.

Merabet L, Desautels A, Minville K, Casanova C (1998) Motion integration in a thalamic visual nucleus. Nature 396:265–268.

Merabet L, Minville K, Ptito M, Casanova C (2000) Responses of neurons in the cat posteromedial lateral suprasylvian cortex to moving texture patterns. Neuroscience 97:611–623.

Miceli D, Repérant J, Ptito M (1985) Intracortical connections of the anterior ectosylvian and lateral suprasylvian visual areas in the cat. Brain Res 347:291–298.

Minville K, Merabet L, Desautels A, Marois A, Casanova C (1997) Response properties of cells in the cat's AMLS cortex. Soc Neurosci Abstr 23 (406):9.

Morrone MC, Di Stefano M, Burr DC (1986) Spatial and temporal properties of neurons of the lateral suprasylvian cortex of the cat. J Neurophysiol 56:969–986.

Movshon JA, Adelson EH, Gizzi MS, Newsome WT (1986) The analysis of moving visual patterns. In: Pattern recognition mechanisms (Chagas C, Gattass R, Gross C, eds), pp 148–164. New York: Springer Verlag.

Norita M, Kase M, Hoshino K, Meguro R, Funaki S, Hirano S, McHaffie JG (1996) Extrinsic and intrinsic connections of the cat's lateral suprasylvian visual area. Prog Brain Res 112:231–250.

Norita M, Mucke L, Benedek G, Albowitz B, Katoh Y, Creutzfeldt OD (1986) Connections of the anterior ectosylvian visual area (AEV). Exp Brain Res 62:225–240.

Olson CR, Graybiel AM (1987) Ectosylvian visual area of the cat: location, retinotopic organization, and connections. J Comp Neurol 261:277–294.

Ouellette BG, Minville K, Faubert J, Casanova C (2001) Motion processing in the AMLS cortex: evidence of a functional differentiation along the medial lateral suprasylvian area. Soc Neurosci Abstr 27 (165):2.

Palmer LA, Rosenquist AC, Tusa RJ (1978) The retinotopic organization of lateral suprasylvian visual areas in the cat. J Comp Neurol 177:237–256.

Raczkowski D, Rosenquist AC (1983) Connections of the multiple visual cortical areas with the lateral posterior-pulvinar complex and adjacent thalamic nuclei in the cat. J Neurosci 3:1912–1942.

Rauschecker JP (1988) Visual function of the cat's LP/LS subsystem in global motion processing. Prog Brain Res 75:95–108.

Rauschecker JP, von Grünau MW, Poulin C (1987) Centrifugal organization of direction preferences in the cat's lateral suprasylvian visual cortex and its relation to flow field processing. J Neurol 7:943–958.

Reinoso-Suárez F, Roda JM (1985) Topographical organization of the cortical afferent connections to the cortex of the anterior ectosylvian sulcus in the cat. Exp Brain Res 59:313–324.

Sanides F, Hoffmann J (1967) Cyto- and myeloarchitecture of the visual cortex of the cat and of the surrounding integration cortices. J Hirnforschung 9:225–252.

Scannell JW, Sengpiel F, Tovée MJ, Benson PJ, Blakemore C, Young MP (1996) Visual motion processing in the anterior ectosylvian sulcus of the cat. J Neurophysiol 76:895–907.

Sherk H (1986) Location and connections of visual cortical areas in the cat's suprasylvian sulcus. J Comp Neurol 247:1–31.

Shipp S, Grant S (1991) Organization of reciprocal connections between area 17 and the lateral suprasylvian area of cat visual cortex. Vis Neurosci 6:339–355.

Skottun BC, De Valois RL, Grosof DH, Movshon JA, Albrecht DG, Bonds AB (1991) Classifying simple and complex cells on the basis of response modulation. Vision Res 31:1079–1086.

Sokal RR, Rohlf FJ (1981) Biometry, 2nd edition, pp 561–690. New York: W. H. Freeman and Company.

Spear PD (1991) Functions of extrastriate visual cortex in non-primate species. In: The neural basis of visual function (Leventhal AG, ed), pp 339–370. London: Macmillan Press.

Spear PD, Baumann TP (1975) Receptive-field characteristics of single neurons in lateral suprasylvian visual area of the cat. J Neurophysiol 38:1403–1420.

Sprague JM, De Weerd P, Xiao D-K, Vandenbussche E, Orban GA (1996) Orientation discrimination in the cat: its cortical locus: II. Extrastriate cortical areas. J Comp Neurol 364:32–50.

Symonds LL, Rosenquist AC (1984a) Corticocortical connections among visual areas in the cat. J Comp Neurol 229:1–38.

Symonds LL, Rosenquist AC (1984b) Laminar origins of visual corticocortical connections in the cat. J Comp Neurol 229:39–47.

Symonds LL, Rosenquist AC, Edwards SB, Palmer LA (1981) Projections of the pulvinar-lateral posterior complex to visual cortical areas in the cat. Neuroscience 6:1995–2020.

Tong L, Kalil RE, Spear PD (1982) Thalamic projections to visual areas of the middle suprasylvian sulcus in the cat. J Comp Neurol 212:103–117.

Toyama F, Fujii K, Umetani K (1990) Functional differentiation be-

tween the anterior and posterior Clare-Bishop cortex of the cat. Exp Brain Res 81:221–233.
Updyke BV (1981) Projections from visual areas of the middle suprasylvian sulcus onto the lateral posterior complex and adjacent thalamic nuclei. J Comp Neurol 201:477–506.
van der Gucht E, Vandesande F, Arckens L (2001) Neurofilament protein: a selective marker for the architectonic parcellation of the visual cortex in adult cat brain. J Comp Neurol 441:345–368.
Vanduffel W, Vandenbussche E, Singer W, Orban GA (1997) A metabolic study of orientation discrimination and detection tasks in the cat. Eur J Neurol 9:1314–1328.
Villeneuve MY, Casanova C (2001) Complex motion integration in cat PMLS cortex. Soc Neurosci Abstr 27 (165):1.
Yaka R, Notkin N, Yinon U, Wollberg Z (2002) Visual, auditory and bimodal activity in the banks of the lateral suprasylvian sulcus of the cat. Neurosci Behav Physiol 32:103–108.
Zumbroich TJ, Blakemore C (1987) Spatial and temporal selectivity in the suprasylvian visual cortex of the cat. J Neurosci 7:482–500.
Zumbroich TJ, von Grünau M, Poulin C, Blakemore C (1986) Differences of visual field representation in the medial and lateral banks of the suprasylvian cortex (PMLS/PLLS) of the cat. Exp Brain Res 64:77–93.

(Accepted 5 September 2003)